A Discrete Memristive Hopfield Neural Network With Grid Multi-structure/scroll-like Attractors

Gang Yang, Chunhua Wang, Yichuang Sun *Senior Member, IEEE*, Quanli Deng

***Abstract*—In constructing memristive neural networks, memristors' intrinsic memory and synapse plasticity characteristics endow the neural networks with complex nonlinear dynamics. However, discrete memristive neural networks with grid multi-structure/scroll-like attractors have not been reported. In this work, a novel discrete memristive Hopfield neural network (DMHNN) is presented by coupling a discrete memristor simulating the mutual synapse into a Hopfield neural network. Multi-structure/scroll-like hyperchaotic attractors are revealed under the control of coupling strength. Interestingly, by adjusting the network parameters, the system can generate diverse grid-structure/scroll-like attractors with different arrangements, which is a chaotic behavior that previous discrete neural networks do not possess. For different sets of network parameters, DMHNN can exhibit multidirectional initial offset-boosting phenomena and can control an arbitrary number of coexisting homogeneous attractors. FPGA-based hardware circuit is designed, and grid multi-structure/scroll-like attractors are successfully implemented. Furthermore, DMHNN is applied to a pseudo-random number generator (PRNG) to evaluate its randomness performance.**

***Index Terms*—Discrete memristor, Hopfied neural network, grid multi-structure/scroll-like attractors, initial offset-boosting, PRNG.**

I. Introduction

AS the fourth basic circuit element, the memristor holds an important position in the field of new electronic devices due to its unique synapse-like and memory characteristics [1]. This component not only provides the physical realization foundation for in-memory computing architectures [2] and neuromorphic engineering [3], but also demonstrates its distinct advantages in scenarios such as chaotic encryption [4], [5] and secure communication [6], [7]. In recent years, the study of memristors has expanded from the continuous domain to the discrete domain. Compared to continuous memristors, discrete memristors applied to low-dimensional chaotic maps exhibit superior dynamical complexity and realize complicated chaotic oscillations with simpler structures [8], [9]. Besides, their mathematical representation makes them particularly prominent in terms of digital system compatibility [10], [11]. Consequently, discrete memristors have become a central topic in the field of nonlinear dynamics theory and artificial neural networks [12]–[14]. Lai et al [15] introduced four ideal discrete memristors, and four hyperchaotic maps were constructed by adding an oscillatory term to them. The complicated dynamical behaviors were found, including coexisting bistable attractors, symmetrically coexisting attractors, and coexisting homogeneous and heterogeneous attractors. Li et al [16] proposed a 2-lobe discrete corsage memristor characterized by the nonvolatility, bistability, and odd-symmetric locally active region. The neuron map coupled by this memristor exhibits multiple symmetric periodic and chaotic attractors, as well as offset-boosted coexistence behaviors. Yuan et al [17] constructed high-dimensional discrete memristive maps with different topologies by coupling multiple discrete memristors, significantly improving parameter space and chaotic range.

Research on the information processing mechanism of neural networks based on the dynamics perspective provides a key entry point for revealing the essential laws of human brain cognition [18], [19]. With the flourishing development of computational neuroscience, a series of artificial neural network models grounded in the electrophysiological properties of biological neurons emerged one after another. Among them, the Hopfield neural network (HNN) distinguished itself as a paradigmatic research subject in both neuroscience and nonlinear dynamics, owing to its distinctive associative memory mechanism and characteristics of global stability. Lin et al [20] presented a memristive HNN with three memristive systems, which can produce grid multi-butterfly attractors and plane coexisting multi-butterfly attractors under the combined action of three memristors. Zhang et al [21] coupled the memristors with a HNN, and a multidirectional multidouble-scroll memristive HNN with countless coexisting multidouble scroll attractors was constructed. Yu et al [22] introduced a novel four-dimensional fractional-order memristive HNN to simulate induced current, demonstrating the dynamics of transient chaos and coexisting attractors. Discrete chaotic maps have low time consumption and show chaos and hyperchaos in low dimensions [23]. Therefore, discrete HNNs have also attracted the attention of researchers. Bao et al [24] proposed a discrete two-neuron HNN with sine activation functions, and special polyhedral hyperchaotic attractors were discovered. Bao et al [25] constructed a two-heterogeneous-neuron HNN with multifolded hyperchaotic attractors by further exploring the two-dimensional discrete HNN. Wei et al [26] employed a discrete memristor to mimic a self-synapse and added it into a two-dimensional HNN, resulting in the appearance of multi-ringlike attractors, hyperchaos, periodic offset, and coexistence of infinite attractors. Bao et al [27] integrated a discrete memristor with a multi-segment state function into a two-

Manuscript received Month xx, 2xxx; revised Month xx, xxxx; accepted Month x, xxxx. This work was supported in part by the National Natural Science Foundation of China under Grants 62571183 and 62271197, and in part by the Guangdong Basic and Applied Basic Research Foundation under Grant 2024A1515011910.

Gang Yang, Chunhua Wang, and Quanli Deng are with the College of Information Science and Engineering, Hunan University, Changsha, 410082, China (Corresponding author: Chunhua Wang, e-mail: wch1227164@hnu.edu.cn).

Chunhua Wang is also with the Greater Bay Area Institute for Innovation, Hunan University, Guangzhou, 511300, China.

Yichuang Sun is with the School of Engineering and Computer Science, University of Hertfordshire, Hatfield AL10 9AB, U.K.

neuron HNN, which is capable of producing multi-stripe/wave hyperchaotic attractors, and also has different numbers of coexisting attractors.

Existing research demonstrates that continuous multi-scroll/multi-structure attractors [28], [29] can be generated through the strategic incorporation of additional 2-index saddle-focus equilibrium points within the system, typically implemented via piecewise nonlinear functions or functionally equivalent memristive elements. Compared to multi-scroll attractors, the topology of multi-structure attractors is irregularly shaped, which makes their phase trajectories more intricate, thus multi-structure attractors have a higher dynamical complexity [29]. In the discrete domain, we have also identified the existence of attractors similar to continuous multi-scroll/structure attractors. So far, discrete multi-cavity attractors [30], multi-vortex-like attractors [31], multi-layer attractors [32], multi-ringlike attractors [26], and multi-stripe/wave attractors [27] have been uncovered. However, these discrete attractors only produce multiple attractors in a single direction without the control of external functions. The complicated discrete grid attractors have still not been reported in neural networks. Therefore, it is particularly important to construct a discrete neural network with grid multi-structure/scroll-like attractors.

Inspired by the above outline, this paper presents a discrete memristive HNN, which is constructed by coupling a discrete cosine memristor to a two-neuron HNN. The system can generate diverse grid multi-structure/scroll-like attractors, and exhibit multidirectional initial offset-boosting behavior, including 1-direction, 2-direction, and 3-direction.

The main contributions of this work are summarized as follows:

1) A novel DMHNN is proposed by coupling a discrete cosine memristor mimicking a mutual synapse into a two-neuron HNN. Theoretical analysis and numerical simulations show that the system is characterized by numerous fixed points, hyperchaos, and state transitions.

2) Under the control of the coupling strength, multi-structure/scroll-like attractors with different topologies are generated. By adjusting the network parameters, rare grid-structure/scroll-like attractors emerge in the phase plane, encompassing both ordered and disordered types.

3) Unlike previous continuous chaotic systems that rely on multiple memristors to achieve multidirectional initial offset-boosting, the system can exhibit this behavior in 1-, 2-, and 3-directions. Moreover, its three-dimensional spatial initial offset capability is absent in existing discrete chaotic systems.

4) The FPGA-based DMHNN hardware circuit was designed, and the experimental results of its grid multi-structure/scroll-like attractors are consistent with the numerical results. In addition, DMHNN is applied to PRNG, and the test results demonstrate that DMHNN can produce high-quality random numbers.

The rest of this paper is organized as follows. Section II presents a discrete memristor and constructs a DMHNN. Section III investigates the Lyapunov exponent (LE) spectra and bifurcation diagrams (BDs) for network parameters, grid multi-structure/scroll-like attractors, and multidirectional initial offset-boosting behavior. Section IV implements the DMHNN hardware circuit using FPGA. Section V designs a DMHNN-based PRNG and evaluates its randomness. Section VI summarizes the paper.

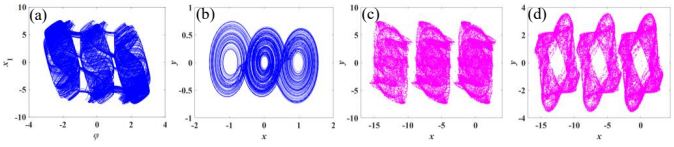

Fig. 1: Multi-structure and multi-scroll attractors in continuous and discrete domains. (a) Continuous 3-structure. (b) Continuous 3-scroll. (c) Discrete 3-structure. (d) Discrete 3-scroll-like.

II. MATHEMATICAL MODELING OF DMHNN

This section describes the difference between multi-structure attractors and multi-scroll attractors. Besides, a three-dimensional DMHNN is constructed by coupling a discrete memristor as a synapse to a discrete bi-neuron Hopfield neural network, and investigates the fixed points and stability of DMHNN.

A. Multi-structure Attractor and Multi-scroll-like Attractor

To verify that multi-structure attractors exhibit more complex dynamics than multi-scroll attractors, we conduct a comparative analysis to elucidate their topological and dynamic trajectory differences. Fig. 1 presents multi-structure and multi-scroll attractors in continuous and discrete domains. Comparing Fig. 1(a) and (b), we can clearly see that the topology of multi-structure attractors is not formed in a scroll shape, and their internal structure is more intricate. Moreover, the phase trajectory of multi-structure attractors exhibits greater randomness within the attractor region and covers a more extensive range. Consequently, multi-structure attractors possess higher dynamical complexity.

This study unveils the existence of multi-structure and multi-scroll-like attractors in the discrete domain, as illustrated in Fig. 1(c) and (d). It can be found that discrete multi-structure attractors have a special topology, and their trajectory jumps randomly between different structures, which is similar to the characteristics of continuous multi-structure attractors. Similarly, discrete multi-scroll-like attractors maintain the fundamental features of continuous multi-scroll attractors.

B. Modeling of Discrete Memristor

In the time domain, the memristors are categorized into continuous and discrete memristors. According to circuit theory completeness, continuous memristors were first defined by Chua, and discrete memristors were obtained by discretizing continuous memristors using the Euler difference method. Based on the state stability, repeatability, and fast computational efficiency of the discrete memristors, we propose a discrete memristor model, which is mathematically defined as follows:

$$\begin{cases} i_n = W(\varphi_n)v_n = \cos(\varphi_n)v_n \\ \varphi_{n+1} = \varphi_n + \eta v_n - \sin(\varphi_n) \end{cases} \tag{1}$$

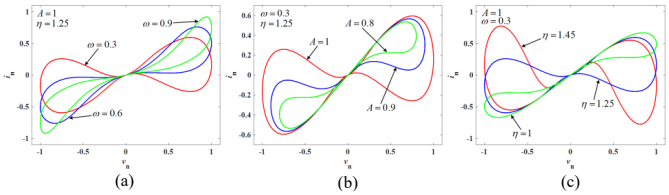

Fig. 2: Voltage-current pinched hysteresis loops of the discrete memristor (1). (a) Frequency-dependent hysteresis loops with $\omega = 0.3$, 0.6, and 0.9. (b) Amplitude-dependent hysteresis loops with $A = 0.8$, 0.9, and 1. (c) Memristor parameter-dependent hysteresis loops with $\eta = 1$, 1.25, and 1.45.

where i_n, v_n, and φ_n denote the n-th iteration values of the discrete current, voltage, and internal state, respectively. $W(\varphi_n) = \cos(\varphi_n)$ represents the discrete memductance, and η is the parameter of the discrete memristor.

A sinusoidal voltage source $v_n = A\sin(\omega n)$ is employed at the input of the discrete memristor (1) to analyze the voltage-current hysteresis hoop of the memristor and validate whether it satisfies the characteristics of the memristor. Fixed $A = 1$ and $\eta = 1.25$, the pinched hysteresis loops related to frequencies $\omega = 0.3$, 0.6, and 0.9 are presented in Fig. 2(a). By selecting $\omega = 0.3$ and $\eta = 1.25$, the hysteresis loops corresponding to amplitudes $A = 0.8$, 0.9, and 1 are depicted in Fig. 2(b). When $A = 1$ and $\omega = 0.3$, the memristor parameter-dependent hysteresis loops for $\eta = 1$, 1.25, and 1.45 are shown in Fig. 2(c). It can be seen from Fig. 2 that the hysteresis loops of the discrete memristor (1) shrink with increasing frequency ω and enlarge with increasing amplitude A, conforming to the definition of the discrete memristors. Meanwhile, the memristor parameter η affects the features of the memristor.

The above results verify that this discrete memristor inherently inherits and maintains the memory, nonlinearity, and synaptic-like characteristics of its continuous counterpart [33]. To construct a discrete memristive neural network with complex dynamic behaviors, this study employs the memristor to emulate a neural synapse and couples it into a discrete Hopfield neural network.

C. Modeling of DMHNN

The discrete Hopfield neural network originates from the discretization of the continuous Hopfield neural network, which is described in mathematical form as:

$$x_i(n+1) = (1 - \frac{h}{C_i R_i})x_i(n) + \frac{h}{C_i}\sum_{j=1}^{n} w_{ij}V_j + \frac{hI_i}{C_i} \quad (2)$$

where h is an iteration step. C_i, R_i, and I_i are the membrane capacitance, the membrane resistance, and the external excitation current, respectively. x_i denotes the membrane potential of neuron i. w_{ij} represents the connection weights between neuron i and neuron j. And V_j is the nonlinear activation functions.

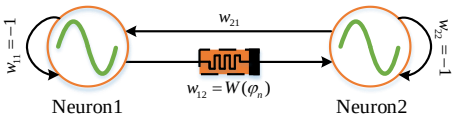

Fig. 3: Specific network topological connection of the DMHNN.

Without loss of generality, $C_i = 1$, $I_i = 0$, and $h = 1$. $\alpha = 1 - \frac{1}{R_i}$, stands for the internal decay. Thus, the discrete Hopfield neural network (2) can be converted to:

$$x_i(n+1) = \alpha x_i(n) + \sum_{j=1}^{n} w_{ij}V_j \quad (3)$$

To explore grid multi-structure/scroll-like attractors in the discrete neural network, we replace the weight from neuron 1 to neuron 2 in the discrete bi-neuron Hopfield neural network by the discrete memristor (1), and the specific network topological connection is shown in Fig. 3. According to the neural network structure in Fig. 3, the model expression of DMHNN can be derived as:

$$\begin{cases} x_{n+1} = \alpha x_n + w_{11}\sin(x_n) + k\sin(y_n)\cos(z_n) \\ y_{n+1} = \beta y_n + w_{21}\sin(x_n) + w_{22}\sin(y_n) \\ z_{n+1} = z_n + \eta\sin(y_n) - \sin(z_n) \end{cases} \quad (4)$$

where the weights w_{11} and w_{22} are both fixed at -1, and k represents the coupling strength. α and β represent the internal decay coefficients of neuron 1 and neuron 2, respectively. To account for the inherent heterogeneity commonly observed among homogeneous neurons in biological neural networks [34], α and β can be assigned different values.

D. Fixed Points and Stability Analysis

The stability of a discrete chaotic map can be determined by analyzing its fixed points. We assume that the fixed point of DMHNN is $P(X, Y, Z)$, then the fixed point P is the solution of the following equation:

$$\begin{cases} X = \alpha X - \sin X + k\sin Y\cos Z \\ Y = \beta Y + w_{21}\sin X - \sin Y \\ Z = Z + \eta\sin Y - \sin Z \end{cases} \quad (5)$$

When the fixed point $P = (0, 0, \xi)$, the equation (5) can be rewritten as:

$$\xi = \xi - \sin\xi \quad (6)$$

apparently, we can compute that $\xi = u\pi$ $(u = 0, \pm1, \pm2, \cdots)$ are the solutions of Eq.(6). As a result, $(0, 0, u\pi)$ are all fixed points of DMHNN.

Set the parameters $\alpha = 1$ and $\beta = 1$, it can be deduced that the fixed points $P = (m\pi, n\pi, l\pi)$, (m, n, and l are integers) are all the solutions of Eq.(5), thus DMHNN has infinite fixed points.

The eigenvalues of the Jacobian matrix at the fixed point determine the stability of the discrete chaotic systems. If all absolute eigenvalues are less than 1, the fixed point is stable; if any absolute eigenvalue greater than 1, the fixed point is

TABLE I: PARAMETERS, FIXED POINTS, EIGENVALUES, AND STABILITY OF DMHNN

Parameters	Fixed Points	Eigenvalues	Stability
$(\alpha, \beta, k, w_{21}, \eta) = (1, 0.5, 2.49, 4, 1.25)$	$(0, 0, u\pi)$, $u = 0, \pm2, \pm4, \cdots$	0, -3.4158, 2.9158	unstable
	$(0, 0, u\pi)$, $u = \pm1, \pm3, \pm5, \cdots$	2,-0.2500 ± 3.1460i	unstable
$(\alpha, \beta, k, w_{21}, \eta) = (1, 1, 2.6, -2.2, 1)$	(0,0,0)	0,0 $\pm$ 2.3917i	stable
	$(\pi, 0, 0)$	0, -1.5923, 3.5923	unstable
	$(0, \pi, 0)$	0, 3.5923, -1.5923	unstable
	$(0, 0, \pi)$	2, 2.3917, -2.3917	unstable
	$\vdots$	$\vdots$	$\vdots$

unstable. Thereby, the Jacobian matrix at the fixed point P can be described as:

$$J_P = \begin{bmatrix} \alpha - \cos X & k\cos Y \cos Z & -k \sin Y \sin Z \\ w_{21}\cos X & \beta - \cos Y & 0 \\ 0 & \eta \cos Y & 1 - \cos Z \end{bmatrix} \quad (7)$$

we solve Eq.(7) using numerical simulation, and the eigenvalues and stability of the Jacobian matrix at these fixed points are listed in Table I.

III. COMPLEX DYNAMICS ANALYSIS

In this section, we systematically investigate the effects of coupling strength k, internal decay coefficient β, weight w_{21}, and memristor internal coefficient η on the system dynamics, and determine appropriate value ranges for these network parameters. Based on these parameter ranges, we conducted fine-grained parameter sampling and adjustment to accurately capture and document a series of newly discovered dynamic phenomena, including grid multi-structure/scroll-like attractors and multidirectional initial offset-boosting behaviors. In the subsequent research, the internal decay coefficient α, weights w_{11}, and w_{22} are fixed to 1, -1, and -1.

A. LE Spectra and BDs for Network Parameters

The network parameters have a significant impact on the dynamics of DMHNN, we set the initial values as $(x_0, y_0, z_0) = (0.1, 0.1, 0.001)$, and investigate the LE spectra and BDs concerning the coupling strength k and internal decay coefficient β. Fig. 4 illustrates the corresponding simulation results, and other network parameter values are marked in detail. For the computation of LEs, we adopted the QR decomposition-based Jacobian matrix method, which is versatile, fast, and numerically accurate [35].

We can discover from Fig. 4 that DMHNN exhibits hyperchaotic behavior under the control of two network parameters. The complicated behaviors of periodic, quasi-periodic, chaotic, and periodic windows are present in Fig. 4(a) and (c). At thesame time, the emergence of anti-period doubling and period doubling can be observed in Fig. 4(c2). Furthermore, the results of Fig. 4(b) and (d) show that the system is in a hyperchaotic state except for the periodic window. The region highlighted by the bright cyan box has the state transition

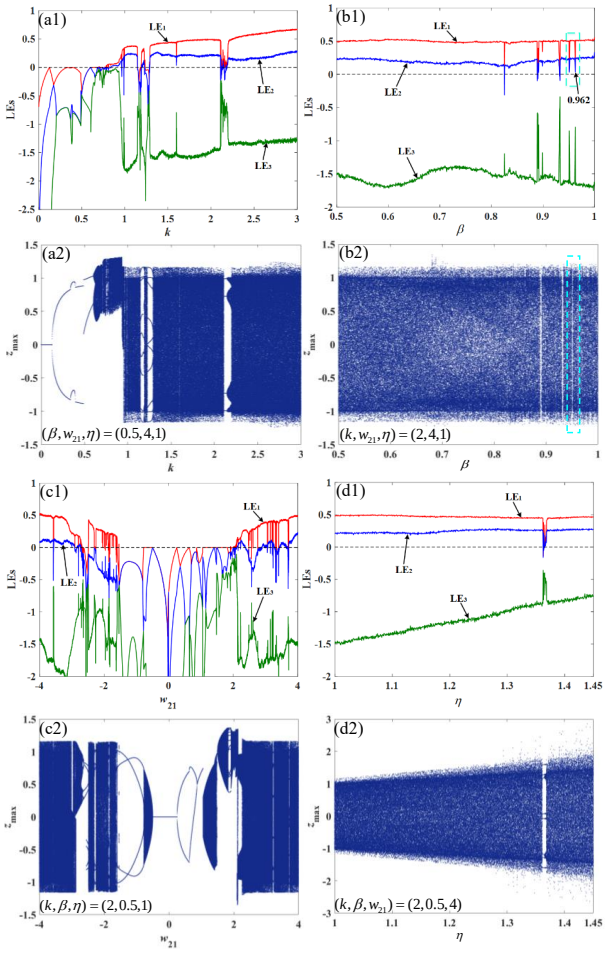

Fig. 4: Network parameter-relied LE spectra and BDs. (a) For $(\beta, w_{21}, \eta) = (0.5, 4, 1)$, numerical simulation plots with $k \in [0, 3]$. (b) For $(k, w_{21}, \eta) = (2, 4, 1)$, numerical simulation plots with $\beta \in [0.5, 1]$. (c) For $(k, \beta, \eta) = (2, 0.5, 1)$, numerical simulation plots with $w_{21} \in [-4, 4]$. (d) For $(k, \beta, w_{21}) = (2, 0.5, 4)$, numerical simulation plots with $\eta \in [1, 1.45]$.

phenomenon in Fig. 4(b). When $\beta = 0.962$ is selected, the corresponding iteration sequence of state variable x and x-z phase portrait are depicted in Fig. 5. The transition from a

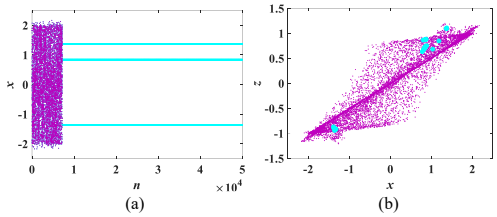

Fig. 5: The x-sequence and x-z phase portrait for $\beta = 0.962$. (a) Iteration sequence of state variable x. (b) x-z phase portrait.

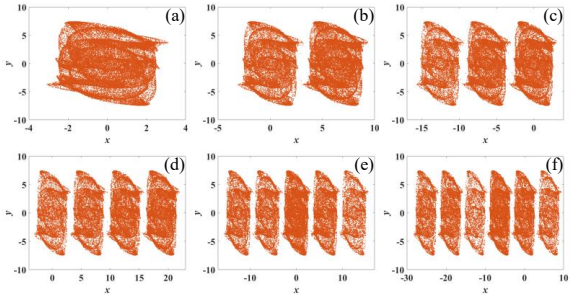

Fig. 6: Multi-structure attractors of the DMHNN with different k values for $(\beta, w_{21}, \eta) = (0.5, 4, 1.25)$ and iteration time $N = 50000$. (a) 1-structure attractor with $k = 2.49$. (b) 2-structure attractor with $k = 2.494$. (c) 3-structure attractor with $k = 2.5$. (d) 4-structure attractor with $k = 2.5012$. (e) 5-structure attractor with $k = 2.5018$. (f) 6-structure attractor with $k = 2.5063$.

chaotic attractor to a periodic state can be clearly seen.

B. Grid Multi-structure/scroll-like Attractors

Fixing the initial values $(x_0, y_0, z_0) = (0.1, 0.1, 0.001)$ and iteration time $N = 50000$, grid multi-structure/scroll-like attractors generated by DMHNN are analyzed by employing phase portraits, LE spectra and BDs, and bi-parameter LE planes. First, we take the parameters as $(\beta, w_{21}, \eta) = (0.5, 4, 1.25)$, and select eight values of the coupling strength k. The multi-structure attractors produced in the x-y plane are present in Fig. 6. As can be seen in Fig. 6, 1-structure to 6-structure attractors are unveiled. Meanwhile, we can also observe that the topology of this type of attractor is solid. Second, the parameters (β, w_{21}, η) are chosen as (1,-2.2,1), the coupling strength k is used as the adjustable parameter, and different numbers of scroll-like attractors are illustrated in Fig. 7. We can see that the structural center of this type of attractor is hollow, which has similar topological feature and dynamic behavior to the continuous multi-scroll attractors. The dynamic properties of these multi-structure/ scroll-like attractors are evaluated as depicted in Fig. 8. From the LE spectra and BD of Fig. 8, it can be concluded that the attractors in Fig. 6 and 7 are hyperchaotic.

Next, when the internal decay $\beta = 0.5$ and the weight $w_{21} = 3$, the grid-structure attractors can be obtained in the x-z plane under different values of the coupling strength k and the memristor parameter η, as shown in Fig. 9. The arrangement of grid-structure attractors in Fig. 9(a)-(c) is ordered,

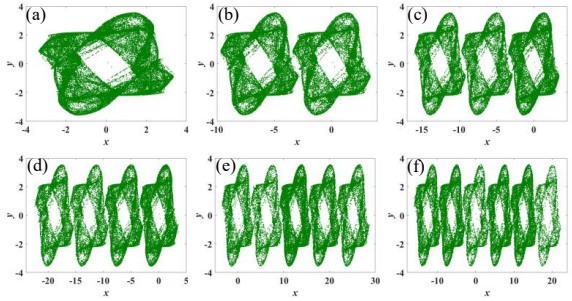

Fig. 7: Multi-scroll-like attractors of the DMHNN with different k values for $(\beta, w_{21}, \eta) = (1, -2.2, 1)$ and iteration time $N = 50000$. (a) 1-scroll-like attractor with $k = 2.6$. (b) 2-scroll-like attractor with $k = 2.613$. (c) 3-scroll-like attractor with $k = 2.617$. (d) 4-scroll-like attractor with k=2.6216. (e) 5-scroll-like attractor with k=2.6241. (f) 6-scroll-like attractor with $k = 2.6253$.

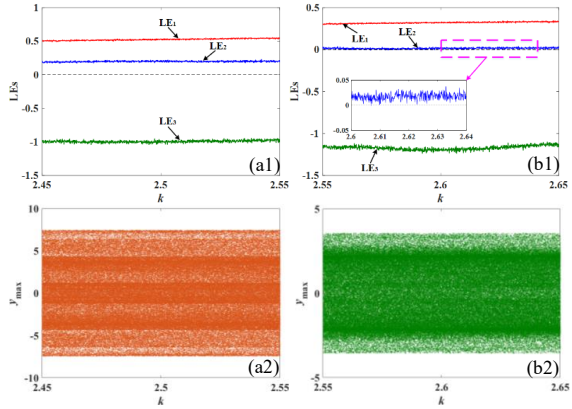

Fig. 8: LE spectra and BDs with respect to k. (a) LE spectrum and bifurcation related to k for $(\beta, w_{21}, \eta) = (0.5, 4, 1.25)$. LE spectrum and bifurcation related to k for $(\beta, w_{21}, \eta) = (1, -2.2, 1)$.

and Fig. 9(d)-(f) exhibit disordered grid-structure attractors. Finally, the parameters (β, w_{21}, η) is set to (1,1.95,1), and the disordered grid-scroll-like attractors appear in the x-y plane under the influence of the coupling strength k, as shown in Fig. 10. Compared to the attractor topology in Fig. 7, the attractor structure of Fig. 10 is evolved, attributed to the variation in network parameters. It is noteworthy that when the iteration time N is further increased to over 50,000, the number of grid multi-structure/scroll-like attractors correspondingly increases. This phenomenon arises from the adopted cosine discrete memristor model and the sine activation function used in the neural network. Unlike chaotic systems that rely on external piecewise-linear functions to generate regular grid attractors by precisely positioning equilibrium points, the disordered grid attractors shown in Figs. 9 and 10 are dynamic outcomes that emerge naturally through the adjustment of network parameters. Due to the system's high sensitivity to parameter variations, its trajectory in phase space undergoes continuous stretching and folding. This dynamic process alters the spatial positions and topological structures of these attractors,

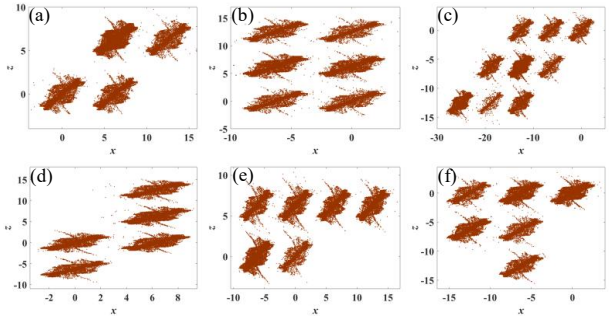

Fig. 9: Grid-structure attractors of the DMHNN with different values of k and η for $(\beta, w_{21}) = (0.5, 3)$ and iteration time $N = 50000$. (a) 2×2-structure attractor with $k = 2.383$ and $\eta = 1.41$. (b) 2×3-structure attractor with $k = 2.398$ and $\eta = 1.41$. (c) 3×3-structure attractor with $k = 2.394$ and $\eta = 1.425$.(d) 1+2+1+1-structure attractor with $k = 2.386$ and $\eta = 1.43$. (e) 2+4-structure attractor with $k = 2.396$ and $\eta = 1.449$. (f) 1+2+3-structure attractor with $k = 2.385$ and $\eta = 1.435$.

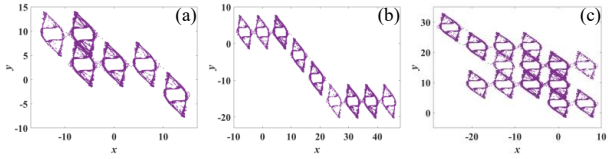

Fig. 10: Grid-scroll-like attractors of the DMHNN with different k values for $(\beta, w_{21}, \eta) = (1, 1.95, 1)$ and iteration time $N = 50000$. (a) 1+3+2-scroll-like attractor with $k = 2.144$. (b) 3+1+1+3-scroll-like attractor with $k = 2.146$. (c) 2+4+4+3+1-scroll-like attractor with $k = 2.15$.

thereby generating such disordered arrangements that reflect the intricate dynamical behavior and parameter sensitivity of DMHNN. Bi-parameter LE maps in Fig. 11(a) display that LE_1 and LE_2 are positive within the parameter ranges of $k \in [2.37, 2.42]$ and $\eta \in [1.4, 1.45]$. This result indicates that grid-structure attractors in Fig. 9 exhibit hyperchaotic characteristics. Furthermore, the LE spectrum and bifurcation diagram with respect to k in Fig. 11(b) confirm that the grid-scroll-like attractors in Fig. 10 are all chaotic.

To summarize, we can detect from Figs. 6 and 7 that the structure attractor traverses a wider range than the scroll-like attractor, deducing that the ergodicity of structure attractors is better. Under the control of only one memristor, the system can produce grid-structure/scroll-like attractors, unlike previous memristive neural networks that required the exertion of multiple memristors or nonlinear functions to achieve the behavior. Additionally, Figs. 6-11 show that the four types of attractors generated by DMHNN reflect complex dynamical characteristics.

C. Multidirectional Initial Offset-boosting Behavior

The initial offset-boosting behavior is a unique multistability phenomenon that makes homogeneous attractors at different positions coexist by changing the initial values [36]. Based on the proposed DMHNN , the system can exhibit

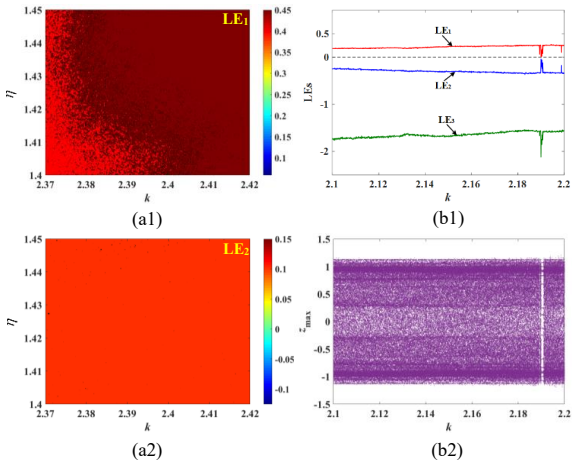

Fig. 11: Dynamical behavior of DMHNN under the network parameters (k, β, w_{21}, η). (a) Bi-parameter LE maps related to k and η for $(\beta, w_{21}) = (0.5, 3)$. (b) LE spectrum and bifurcation related to k for $(\beta, w_{21}, \eta) = (1, 1.95, 1)$.

the initial offset coexistence dynamics in multiple directions for different groups of network parameters. First, when the parameters $(k, \beta, w_{21}\eta) = (2.48, 0.5, 4, 1.25)$ and the initial values $(x_0, y_0, z_0) = (x_0, 0.1, 0.001)$, the structure attractor undergoes the shifting behavior in the x-direction under the influence of x_0, as shown in Fig. 12. Combining the numerical results of the initial value x_0-dependent LE spectrum and BD in Fig. 13, the LE spectrum remains essentially unchanged, and the same blocks of the bifurcation plot are located in the x-direction in a staircase form, which further confirms the initial offset-boosting characteristic. Second, fixing $(k, \beta, w_{21}\eta) = (2, 0.5, 4, 1)$ and $y_0 = 0.1$, attractors with the identical structure coexist in an ordered arrangement within the x-z plane for different values of x_0 and z_0, as depicted in Fig. 14(a). By rationally selecting x_0 and z_0, these attractors can be effectively controlled to distribute in different regions. The basin of attraction in Fig. 14(b) presents the range of initial values corresponding to attractors at the same position. When the initial values x_0 and z_0 are increased by offsets of $2m\pi$ and $2n\pi$, respectively (where m and n are integers), the iterative sequences x and z of the system correspondingly produce offsets of $2m\pi$ and $2n\pi$. This regularity causes attractors with identical topology but different spatial positions to be regularly distributed across the x-z plane, thereby forming the coexistence of homogeneous attractors. Hence, it can be seen that the system can demonstrate the offset phenomenon in the bi-direction. Finally, when the network parameters $(k, \beta, w_{21}, \eta) = (2.5, 1, -2.2, 1)$ are taken, and multiple sets of initial values (x_0, y_0, z_0) are set, scroll-like attractors maintain coexistence in the three dimensional x-y-z space, as illustrated in Fig. 15(a)-(c). This behavior indicates that the system has offset properties in the x, y, and z directions, and the corresponding initial value-related BDs are plotted in Fig. 15(d)-(f), validating the intrinsic tri-directional initial offset-boosting capability of DMHNN.

The multidirectional initial offset-boosting behavior uncovers the coexistence of innumerable homogeneous attractors in

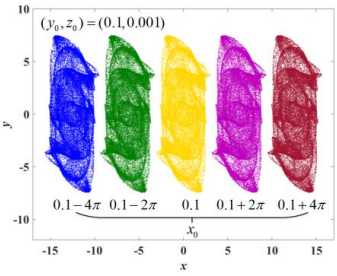

Fig. 12: Uni-directional initial offset-boosting behavior of DMHNN for $(k, \beta, w_{21}, \eta) = (2.48, 0.5, 4, 1.25)$ and $(x_0, y_0, z_0) = (x_0, 0.1, 0.001)$.

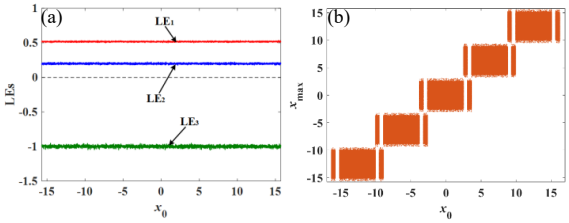

Fig. 13: Initial value x_0-dependent LE spectrum and bifurcation with $(k, \beta, w_{21}, \eta) = (2.48, 0.5, 4, 1.25)$ and $(x_0, y_0, z_0) = (x_0, 0.1, 0.001)$. (a) LE spectrum. (b) BD.

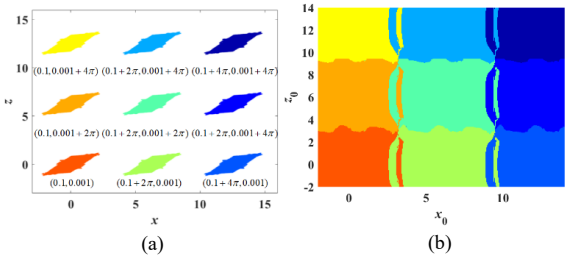

Fig. 14: Bi-directional initial offset-boosting behavior of DMHNN for $(k, \beta, w_{21}, \eta) = (2, 0.5, 4, 1)$ and $y_0 = 0.1$. (a) Coexistence of 3×3 attractors in the x-z plane. (b) Basin of attraction with respect to x_0 and z_0.

multiple directions, further reflecting the intricate coexisting dynamics of DMHNN.

IV. FPGA HARDWARE IMPLEMENTATION

Digital circuits have the advantages of excellent stability, flexibility, reconfigurability, and parallel processing. Notably, discrete chaotic maps possess intrinsic discretized characteristics that render them naturally compatible with digital circuit architectures. To experimentally validate the feasibility of hardware realization for the proposed DMHNN system, we employ FPGA technology to design the hardware circuit. The hardware devices adopted include the Xilinx xc7z020clg400-1 development board, the AD9767 digital-to-analog converter (ADC), and the oscilloscope. In addition, Verilog HDL language is employed for programming in vivado software environment. A 32-bit fixed point format consisting of 1 sign bit, 6 integer bits, and 25 decimal bits defines the network parameters and variables of the DMHNN. The

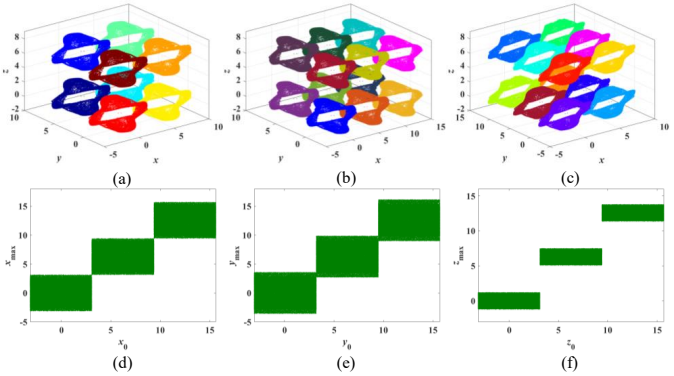

Fig. 15: Tri-directional initial offset-boosting behavior of DMHNN for $(k, \beta, w_{21}, \eta) = (2.5, 1, -2.2, 1)$. (a) Coexistence of $2 \times 2 \times 2$ attractors. (b) Coexistence of $3 \times 2 \times 2$ attractors. (c) Coexistence of $2 \times 3 \times 2$ attractors. (d) Initial value x_0-related BD. (e) Initial value y_0-related BD. (f) Initial value z_0-related BD.

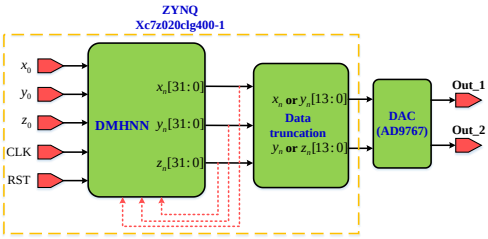

Fig. 16: Overall hardware design flowchart of FPGA-based DMHNN.

overall hardware design flowchart is presented in Fig. 16, where the 32-bit output signals of the DMHNN block must be intercepted into 14-bit digital signals as the input signals of the AD9767 ADC. The final output signals after digital to analog conversion are captured by the oscilloscope and the simulation result of the corresponding attractor is subsequently observed.

This FPGA design operates at a clock frequency of 50 MHz. Under this configuration, a single iteration requires 1840 ns to complete, corresponding to 92 clock cycles. The sine and cosine functions are implemented using the rotation mode of the CORDIC algorithm [37]. Its core is the following unified iterative equation:

$$\begin{cases} U_{i+1} = k_n(U_i - \mu\sigma_i 2^{-i} V_i) \\ V_{i+1} = k_n(V_i + \sigma_i 2^{-i} U_i) \\ W_{i+1} = W_i - \sigma_i \theta_i \end{cases} \tag{8}$$

$$k_n = \prod_{i=0}^{n-1} \sqrt{1 + \mu 2^{-2i}} \tag{9}$$

$$\theta_i = \begin{cases} \arctanh(2^{-i}), \text{if} \mu = -1 \\ 2^{-i}, \text{if} \mu = 0 \\ \arctan(2^{-i}), \text{if} \mu = 1 \end{cases} \tag{10}$$

where k_n denotes the scale factor, and n is the number of iterations. σ_i and θ_i represent the rotation direction and angle value for the i-th iteration, respectively. When computing the sine and cosine functions, μ is set to 1. The algorithm

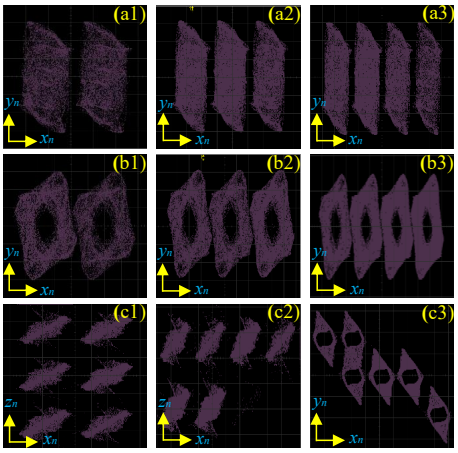

Fig. 17: Hardware experiment results of grid multi-structure/scroll-like attractors. (a) Multi-structure attractors. (b) Multi-scroll-like attractors. (c) Grid-structure/scroll-like attractors.

employs successive pseudo-rotations to make the actual angle progressively approximate the target angle θ. The final outputs for the sine and cosine values are given by $\sin(\theta) \approx V_{n+1}$ and $\cos(\theta) \approx U_{n+1}$.

In the circuit design process, we fixed the initial values as (0.1,0.1,0.001) and selected multiple sets of network parameters as examples. The experiment results of the corresponding multi-structure, grid structure, multi-scroll-like, and grid scroll-like attractors are shown in Fig. 17. Comparing with the numerical results in Figs. 6(b)-(d), 7(b)-(d), 9(b) and (e), and 10(a), it can be seen that they are basically consistent, which confirms the correctness of the FPGA-based DMHNN hardware circuit.

V. APPLICATION IN PRNG

Chaotic signals generated by chaotic systems have unpredictability and initial value sensitivity, which satisfy the construction requirements of PRNG. The core technical indices of PRNG depend on the chaotic system's randomness quality, which is essentially determined by its chaotic dynamics properties. Thus, we select some indicators to evaluate the performance of multi-structure/scroll-like DMHNN (MS/SL-DMHNN), including information entropy (IE), conditional entropy (CE), dispersion entropy (DE), fuzzy entropy (FE) , and Kaplan-Yorke dimension ($\mathrm{D_{KY}}$). In the test process, the length of the chaotic sequence to be estimated is 10000. Table II shows the performance results of MS/SL-DMHNN and other chaotic maps. The parameters and initial values of the MS/SL-DMHNN are selected from configurations capable of generating 3-structure/scroll-like attractors, corresponding to the settings in Fig. 6(c) and Fig. 7(c), respectively. The parameters and initial conditions of the other chaotic maps listed in the table are directly cited from their respective original literature. All models selected for comparison are ensured to be in a verified chaotic or hyperchaotic state. As can be seen from Table II, the chaotic performance of the multi-structure attractor is better than the multi-scroll-like attractor, and the multi-structure attractor has the best entropy indicators in all aspects. Moreover, compared to other chaotic maps, the IE, CE, and FE of MSL-DMHNN are better, and only the DE is smaller than the chaotic maps proposed by reference [12] and [27]. As a result, these evaluation results indicate that MS/SL-DMHNN has good randomness and is suitable for PRNG application.

The number of multi-structure/scroll-like attractors increases along the x-direction, indicating that the x-sequence produced by the system exhibits richer dynamical properties. Therefore, we selected the x-sequences from the MS/SL-DMHNN for the generation of pseudo-random numbers (PRNs), which demonstrates the application potential of these two types of attractors in PRNGs. Before generating PRNs, the system must execute an initialization process: First, DMHNN is pre-run to produce a chaotic sequence $X = \{x_1, x_2, \cdots, x_{n\_pre}\}$ and compute its minimum value $\min(X)$. Subsequently, during the formal PRNG phase, this predefined $\min(X)$ value is used to perform a normalization transformation on each state value x_n $(n = 1, 2, 3, \cdots, n\_pre)$. The required binary sequence P_n is generated by the following equation:

$$P_n = \lfloor M \times (x_n + \mathrm{abs}(\min(X))) \rfloor \bmod N \qquad (11)$$

where $\lfloor \cdot \rfloor$ stands for a downward rounding operation, $M = 10^{11}$, and $N = 2^8$. Hence, each x_n can be converted to an 8-bit binary number P_n, and the subsequent combination of the binary numbers to form PRNs P. The sequence number and length of PRNs P are 128 and 10^6.

To verify that the designed PRNG is capable of generating reliable PRNs, a complete hardware platform was constructed based on the DMHNN hardware circuit implemented in Section IV and the PRNs generation method described by Eq. 11. This platform is illustrated in Fig. 18. The relevant code was programmed using Verilog HDL within the Vivado environment. After synthesis and simulation, it was downloaded to the Xilinx xc7z020clg400-1 chip. Subsequently, the output signal was transmitted to an oscilloscope via the digital-to-analog converter AD9767, ultimately enabling the capture and observation of the generated PRN stream. Fig. 19(a) shows the pseudo-random sequence generated based on this FPGA platform. A comparison with the numerical simulation results in Fig. 19(b) demonstrates a high degree of consistency between the two, successfully achieving the expected PRN stream. Therefore, the experiment confirms that the proposed DMHNN system and the PRNs generation method can effectively produce stable and reliable PRNs on a finite-precision FPGA hardware platform.

In this experiment, we employ the NIST SP800-22 test set for assessing PRNs P. This test set contains 15 evaluation items which are used to detect the randomness and quality of the binary sequences generated by PRNG. The pass rate and P-value$_T$ of each evaluation item measure the randomness of the tested sequence, and a larger P-value$_T$ means that the sequence is more random on this evaluation item. The standard values of pass rate and P-value$_T$ for this test are set at 0.9609 and 0.0001. Furthermore, the parameters and initial values of MS/SL-DMHNN are given in Table II.

TABLE II: PERFORMANCE RESULTS OF DIFFERENT CHAOTIC MAPS

Chaotic Maps	Parameters	Initial Values	IE	CE	DE	FE	D_{KY}
MS-DMHNN	$(k, \beta, w_{21}, \eta) = (2.5, 0.5, 4, 1.25)$	(0.1,0.1,0.001)	5.6321	2.1323	2.1304	1.6624	2.7065
MSL-DMHNN	$(k, \beta, w_{21}, \eta) = (2.617, 1, -2.2, 1)$	(0.1,0.1,0.001)	5.3027	1.8802	2.0125	1.5462	2.2881
Zhang [12]	$(a, b, k_1, k_2) = (0.24, 4, 1, 1)$	(0.1,0.1,0.1)	5.1470	1.7490	2.0629	1.3386	3.0000
Bao [24]	$(\mu, g_{11}, g_{12}, g_{21}, g_{22}) = (0.8, 3, 3, -2, 2)$	(0.1,0.1)	5.0907	1.5771	1.8104	1.1334	2.0000
Wei [26]	$(a, b, k, w_{12}, w_{21}, w_{22}) = (0.5, 0.5, 0.281, -2.75, 2, 2)$	(1,1,1)	4.3066	1.2210	1.8413	0.8971	1.6704
Bao [27]	$(\mu, g_{21}, g_{22}, \varepsilon, M) = (0.5, -4, 4, 0.5, 1)$	$(10^{-6}, 10^{-6}, 0)$	5.0371	1.6875	2.1249	1.4156	2.4150
Fan [31]	$(a_0, a_1, a_2, b_0, b_1, b_2) = (-0.985, 0.83, 0.14, 1.3, 0.1, 1)$	(0.1,0.1,0.1)	4.7525	1.5572	1.8777	0.7563	2.1500
Wang [32]	$(a, b, c, d, k_1, k_2) = (-0.84, -0.1, -0.1, 1, 1.87, 0.37)$	(-1,0,1)	5.2550	1.7808	1.9436	1.2720	2.1517

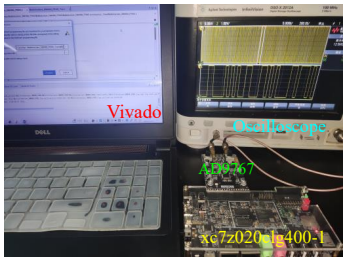

Fig. 18: PRNG implementation based on an FPGA hardware platform.

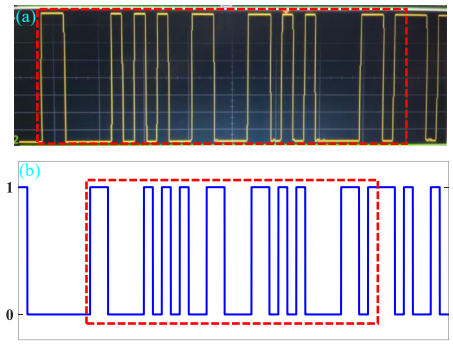

Fig. 19: Comparison of PRNs generated by an FPGA hardware platform and numerical simulation. (a) Results from FPGA hardware implementation. (b) Results from numerical simulation.

TABLE III: NIST TEST RESULTS OF THE PRNs GENERATED BY MS/SL-DMHNN

No.	Sub-tests	MS-DMHNN		MSL-DMHNN	
		Pass rate	P-value$_T$	Pass rate	P-value$_T$
01	Frequency	1.0000	0.3925	0.9844	0.5681
02	Block Frequency	1.0000	0.8043	1.0000	0.7231
03	Cum. Sums*(F)	0.9922	0.6025	0.9766	0.2229
	Cum. Sums*(R)	1.0000	0.9220	0.9844	0.7061
04	Runs	0.9922	0.4686	0.9922	0.3641
05	Longest Runs	0.9844	0.2536	0.9766	0.8486
06	Rank	1.0000	0.2229	0.9922	0.3242
07	FFT	0.9922	0.2328	1.0000	0.0034
08	Non-Ovla. Temp.*	0.9895	0.4285	0.9902	0.4296
09	Ovla. Temp.	0.9922	0.6545	1.0000	0.6025
10	Universal	1.0000	0.2873	0.9844	0.8043
11	Appr. Entropy	0.9922	0.1223	1.0000	0.5681
12	Ran. Exc.*	0.9969	0.4760	0.9918	0.4223
13	Ran. Exc. Var.*	0.9944	0.5391	0.9978	0.3001
14	Serial(1st)	0.9766	0.2041	0.9922	0.5174
	Serial(2nd)	0.9766	0.6198	0.9922	0.6371
15	Linear complexity	0.9922	0.3505	0.9844	0.8623
	Success No.	15/15	15/15	15/15	15/15

Note: *The average result of multiple subtests is reported.

Table III lists the test results of MS/SL-DMHNN PRNG. It can be observed that the pass rate and P-value$_T$ of the two evaluated sequences are greater than the standard values. This implies that MS/SL-DMHNN has complicated chaotic dynamics and generates high-quality randomness numbers. Therefore, the proposed DMHNN can be further applied to secure communication, image encryption, and video encryption.

VI. Conclusion

This paper integrates a novel consine discrete memristor into a Hopfield neural network, whereby a three-dimensional discrete memristive Hopfield neural network is proposed. Theoretical analysis yields that DMHNN has countless fixed points. LE spectra and BDs for network parameters are studied, demonstrating the hyperchaotic and state transition behavior. Different numbers of structure/scroll-like hyperchaotic attractors are generated by adjusting the coupling strength k. Under the influence of only one memristor, complex grid-structure hyperchaos and grid-scroll-like chaos emerge in the phase plane. It is more flexible and resource-efficient than the method of coupling multiple memristors and imposing external nonlinear functions. By modifying the network parameters, the initial offset-boosting behavior is revealed in the single, double, and triple directions. Numerical simulations confirm the coexistence of numerous homogeneous attractors in multiple directions. To verify the feasibility of the hardware implementation, the DMHNN hardware circuit is constructed using FPGA, and the experimental results are in agreement with the numerical results. Besides, DMHNN is employed in PRNG, where multi-structure/scroll-like hyperchaotic sequences are evaluated in the NIST test set, and its results indicate that DMHNN can produce high-quality random numbers. In future

work, we apply DMHNN in practical engineering scenarios, such as secure communication, data encryption transmission, and image encryption. Meanwhile, we will further explore high-dimensional multi-structure discrete memristive neural network with multiple positive LEs.

REFERENCES

[1] X. Zhang, C. Li, T. Lei, H. H.-C. Iu, and T. Kapitaniak, "Coexisting hyperchaos in a memristive neuromorphic oscillator," *IEEE Transactions on Computer-Aided Design of Integrated Circuits and Systems*, vol. 44, no. 8, pp. 3179–3188, 2025.

[2] Y.-H. Ren, S. Yang, J.-H. Bi, and Y.-X. Zhang, "Accelerating maximum-likelihood detection in massive MIMO: A new paradigm with memristor crossbar based in-memory computing circuit," *IEEE Transactions on Vehicular Technology*, vol. 73, no. 12, pp. 19 745–19 750, 2024.

[3] Q. Deng, C. Wang, Y. Sun, X. Cong, H. Lin, and Z. Deng, "Memristor-based brain emotional learning neural network with attention mechanism and its application," *IEEE Transactions on Computer-Aided Design of Integrated Circuits and Systems*, vol. 44, no. 12, pp. 4701–4713, 2025.

[4] F. Yu, S. He, W. Yao, S. Cai, and Q. Xu, "Bursting firings in memristive hopffeld neural network with image encryption and hardware implementation," *IEEE Transactions on Computer-Aided Design of Integrated Circuits and Systems*, vol. 44, no. 12, pp. 4564–4576, 2025.

[5] Q. Deng, C. Wang, and G. Yang, "Discrete memristor-based complex-valued chaotic system dynamics and application in dual-image encryption," *Acta Physica Sinica*, pp. 1–24, 2025.

[6] G. Yang, C. Wang, Y. Sun, and Q. Deng, "A discrete memristive heterogeneous Hopfield neural network with multi-penguin-like/silkworm-like attractors and its application in secure communication," *Nonlinear Dynamics*, 2025.

[7] Q. Deng, C. Wang, G. Yang, and D. Luo, "Discrete memristive delay feedback Rulkov neuron model: Chaotic dynamics, hardware implementation and application in secure communication," *IEEE Internet of Things Journal*, vol. 12, no. 13, pp. 25 559–25 567, 2025.

[8] Q. Lai and L. Yang, "A new 3-D memristive hyperchaotic map with multi-parameter-relied dynamics," *IEEE Transactions on Circuits and Systems II: Express Briefs*, vol. 70, no. 4, pp. 1625–1629, 2022.

[9] L. Ren, J. Mou, S. Banerjee, and Y. Zhang, "A hyperchaotic map with a new discrete memristor model: Design, dynamical analysis, implementation and application," *Chaos, Solitons & Fractals*, vol. 167, p. 113024, 2023.

[10] Q. Deng, C. Wang, Y. Sun, and G. Yang, "Delay difference feedback memristive map: Dynamics, hardware implementation, and application in path planning," *IEEE Transactions on Circuits and Systems I: Regular Papers*, vol. 72, no. 12, pp. 7993–8003, 2025.

[11] D. Luo, C. Wang, Q. Deng, and G. Yang, "Discrete memristive hyperchaotic maps with high lyapunov exponents," *Nonlinear Dynamics*, vol. 113, pp. 28 381–28 395, 2025.

[12] S. Zhang, P. Ma, H. Zhang, H. Lin, and C. Wang, "Dual memristors-radiated discrete Hopfield neuron with complexity enhancement," *Nonlinear Dynamics*, vol. 113, no. 3, pp. 2667–2688, 2025.

[13] H. Li and F. Min, "Large-scale memrisitive Rulkov ring-star neural network with complex spatio-temporal dynamics," *IEEE Transactions on Industrial Informatics*, vol. 20, no. 8, pp. 10 259–10 268, 2024.

[14] D. Luo, C. Wang, J. Liang, and Q. Deng, "Memristor coupled fractional-order Hopfield neural network composed by heterogeneous neurons and its FPGA implementation," *Nonlinear Dynamics*, vol. 113, pp. 29 983–29 998, 2025.

[15] Q. Lai, L. Yang, and G. Chen, "Two-dimensional discrete memristive oscillatory hyperchaotic maps with diverse dynamics," *IEEE Transactions on Industrial Electronics*, vol. 72, no. 1, pp. 969–979, 2024.

[16] H. Li and F. Min, "Attractor dynamics of 2-lobe discrete corsage memristor-coupled neuron map," *IEEE Transactions on Circuits and Systems I: Regular Papers*, vol. 72, no. 9, pp. 4820–4829, 2024.

[17] F. Yuan, S. Zhang, G. Xing, and Y. Deng, "Parameter control methods for discrete memristive maps with network structure," *IEEE Transactions on Industrial Informatics*, vol. 20, no. 5, pp. 7194–7204, 2024.

[18] B. Hu, Z.-H. Guan, G. Chen, and C. P. Chen, "Neuroscience and network dynamics toward brain-inspired intelligence," *IEEE Transactions on Cybernetics*, vol. 52, no. 10, pp. 10 214–10 227, 2021.

[19] G. Yang, C. Wang, Y. Sun, and Q. Deng, "Delayed discrete memristive ring neural network and application in pseudorandom number generator," *IEEE Internet of Things Journal*, 2025.

[20] H. Lin, X. Deng, F. Yu, and Y. Sun, "Grid multi-butterfly memristive neural network with three memristive systems: Modeling, dynamic analysis, and application in police IoT," *IEEE Internet of Things Journal*, vol. 11, no. 18, pp. 29 879–29 889, 2024.

[21] S. Zhang, C. Chen, Y. Zhang, J. Cai, X. Wang, and Z. Zeng, "Multi-directional multidouble-scroll Hopfield neural network with application to image encryption," *IEEE Transactions on Systems, Man, and Cybernetics: Systems*, vol. 55, no. 1, pp. 735–746, 2024.

[22] F. Yu, S. Zhang, D. Su, Y. Wu, Y. M. Gracia, and H. Yin, "Dynamic analysis and implementation of fpga for a new 4D fractional-order memristive hopfield neural network," *Fractal and Fractional*, vol. 9, no. 2, p. 115, 2025.

[23] Y. Zhang, H. Bao, Z. Hua, and H. Huang, "Two-dimensional exponential chaotic system with hardware implementation," *IEEE Transactions on Industrial Electronics*, vol. 70, no. 9, pp. 9346–9356, 2022.

[24] B. Bao, H. Tang, Y. Su, H. Bao, M. Chen, and Q. Xu, "Two-dimensional discrete bi-neuron Hopfield neural network with polyhedral hyperchaos," *IEEE Transactions on Circuits and Systems I: Regular Papers*, vol. 71, no. 12, pp. 5907–5918, 2024.

[25] H. Bao, M. Xi, H. Tang, X. Zhang, Q. Xu, and B. Bao, "Discrete two-heterogeneous-neuron HNN and chaos-based hardware poisson encoder," *IEEE Transactions on Industrial Informatics*, vol. 21, no. 2, pp. 1862–1871, 2024.

[26] Y. Wei, B. Du, X. Wang, Z. Fan, and X. Sun, "Multi-ringlike volumes and offset of Hopfield neural networks based on a discrete memristive self-synapse," *Nonlinear Dynamics*, vol. 113, no. 3, pp. 2729–2746, 2025.

[27] H. Bao, R. Wang, H. Tang, M. Chen, and B. Bao, "Discrete memristive Hopfield neural network with multi-stripe/wave hyperchaos," *IEEE Internet of Things Journal*, vol. 12, no. 12, pp. 20 902–20 912, 2025.

[28] Q. Lai, L. Yang, G. Hu, Z.-H. Guan, and H. H.-C. Iu, "Constructing multiscroll memristive neural network with local activity memristor and application in image encryption," *IEEE Transactions on Cybernetics*, vol. 54, no. 7, pp. 4039–4048, 2024.

[29] H. Lin, C. Wang, C. Xu, X. Zhang, and H. H. Iu, "A memristive synapse control method to generate diversified multistructure chaotic attractors," *IEEE transactions on computer-aided design of integrated circuits and systems*, vol. 42, no. 3, pp. 942–955, 2022.

[30] X. Liu, K. Sun, H. Wang, and S. He, "A class of novel discrete memristive chaotic map," *Chaos, Solitons & Fractals*, vol. 174, p. 113791, 2023.

[31] Z. Fan, X. Sun, J. Zhao, C. Zhang, and B. Du, "Dynamics analysis and feasibility verification of a 3D discrete memristive chaotic map with multi-vortex-like volume behavior," *Chaos, Solitons & Fractals*, vol. 185, p. 115070, 2024.

[32] X. Wang, Y. Wei, X. Sun, Z. Fan, and B. Du, "A novel discrete memristive hyperchaotic map with multi-layer differentiation, multi-amplitude modulation, and multi-offset boosting," *Chaos: An Interdisciplinary Journal of Nonlinear Science*, vol. 34, no. 11, 2024.

[33] H. Bao, Z. Hua, H. Li, M. Chen, and B. Bao, "Discrete memristor hyperchaotic maps," *IEEE Transactions on Circuits and Systems I: Regular Papers*, vol. 68, no. 11, pp. 4534–4544, 2021.

[34] F. Baroni and A. Mazzoni, "Heterogeneity of heterogeneities in neuronal networks," *Frontiers in computational neuroscience*, vol. 8, p. 161, 2014.

[35] K. Geist, U. Parlitz, and W. Lauterborn, "Comparison of different methods for computing lyapunov exponents," *Progress of theoretical physics*, vol. 83, no. 5, pp. 875–893, 1990.

[36] Q. Wan, Q. Yang, T. Liu, C. Chen, and K. Shen, "Single direction, grid and spatial multi-scroll attractors in Hopfield neural network with the variable number memristive self-connected synapses," *Chaos, Solitons & Fractals*, vol. 189, p. 115584, 2024.

[37] S. M. Mohamed, W. S. Sayed, A. G. Radwan, and L. A. Said, "FPGA implementation of reconfigurable CORDIC algorithm and a memristive chaotic system with transcendental nonlinearities," *IEEE Transactions on Circuits and Systems I: Regular Papers*, vol. 69, no. 7, pp. 2885–2892, 2022.

Chunhua Wang received the M.S. degree in microphysics from Zhengzhou University, Zhengzhou, China, in 1994, and the Ph.D. degree in microelectronics and solid-state electronics from Beijing University of Technology, Beijing, China, in 2003.

He is currently a Professor with the College of Computer Science and Electronic Engineering, Hunan University, Changsha, China, where he is also a Doctor Tutor and the Director of the Advanced Communication Technology Key Laboratory. He has presided over more than eight national and provincial projects and authored or co-authored more than 200 articles retrieved by SCI, among which 20 articles were highly cited. His research interests include chaotic circuits, memristor circuits, chaotic encryption, neural networks based on memristor, complex networks, and current-mode circuits.

Dr. Wang is the Director of the Chaos and Nonlinear Circuit Professional Committee of the Circuit and System Branch of the China Electronic Society.

Yichuang Sun (Senior Member, IEEE) received the B.Sc. and M.Sc. degrees from Dalian Maritime University, Dalian, China, in 1982 and 1985, respectively, and the Ph.D. degree from the University of York, York, U.K., in 1996, all in communications and electronics engineering.

Dr. Sun is currently Professor of Communications and Electronics, Head of Communications and Intelligent Systems Research Group, and Head of Electronic, Communication and Electrical Engineering Division in the School of Engineering and Computer Science of the University of Hertfordshire, UK. He has published over 420 papers and contributed 10 chapters in edited books. He has also published four text and research books: Continuous-Time Active Filter Design (CRC Press, USA, 1999), Design of High Frequency Integrated Analogue Filters (IEE Press, UK, 2002), Wireless Communication Circuits and Systems (IET Press, 2004), and Test and Diagnosis of Analogue, Mixed-signal and RF Integrated Circuits - the Systems on Chip Approach (IET Press, 2008). His research interests are in the areas of wireless and mobile communications, RF and analogue circuits, memristor circuits and systems, and machine learning and neuromorphic computing.

Gang Yang received the B.S. degree in communications engineering and the M.S. degree in artificial intelligence form the Jiangxi University of science and technology, Ganzhou, China, in 2020 and 2023, respectively. He is currently pursuing the Ph.D degree with the college of computer science and electronic engineering, Hunan University, Changsha, China.

His current research interests include chaotic systems and circuits, memristor neural networks, and memristor systems and circuits.

Quanli Deng received the B.S. degree in microelectronics from the School of Physics and Optoelectronics, Xiangtan University, Xiangtan, China, in 2016, and the M.S. degree in information and communication engineering and the Ph.D. degree in computer science and technology from the College of Computer Science and Electronic Engineering, Hunan University, Changsha, China, in 2020 and 2024, respectively.

He is currently a Post-Doctoral Research Fellow with the College of Computer Science and Electronic Engineering, Hunan University. His research interests include modeling and analysis of neural systems, fundamental theory of nonlinear systems and circuits, and analog implementation of neuromorphic systems.